Journal of
Synchrotron Radiation

ISSN 0909-0495

Received 10 March 2011
Accepted 21 June 2011

Application of X-ray fluorescence to turbulent mixing

Alan Kastengren,[a]* Christopher F. Powell,[a] Eric M. Dufresne[b] and Donald A. Walko[b]

[a]Energy Systems Division, Argonne National Laboratory, 9700 South Cass Avenue, Argonne, IL 60439, USA, and [b]X-ray Science Division, Advanced Photon Source, Argonne National Laboratory, Argonne, IL 60439, USA. E-mail: akastengren@anl.gov

Combined measurements of X-ray absorption and fluorescence have been performed in jets of pure and diluted argon gas to demonstrate the feasibility of using X-ray fluorescence to study turbulent mixing. Measurements show a strong correspondence between the absorption and fluorescence measurements for high argon concentration. For lower argon concentration, fluorescence provides a much more robust measurement than absorption. The measurements agree well with the accepted behavior of turbulent jets.

Keywords: fluorescence spectroscopy; X-ray absorption; turbulent flow.

1. Introduction

To avoid the introduction of intrusive probes in turbulent flows, a wide variety of optical flow diagnostics have been developed. In flows that are optically dense, these techniques can have severe limitations, necessitating the use of alternative diagnostics. For example, multiple-scattering effects in optically dense spray flowfields can make quantitative optical diagnostics highly problematic (Sick & Stojkovic, 2001). X-rays scatter from materials much less readily than visible light, making X-ray techniques attractive in multiphase flowfields. X-ray radiography has been used to quantitatively probe dense multiphase flowfields under a variety of conditions (Kastengren *et al.*, 2009; MacPhee *et al.*, 2002; Kuo *et al.*, 1990).

A limitation of radiography for weakly absorbing samples is the requirement to measure a small decrement of the X-ray intensity. This signal is easily corrupted by noise or drifts between the detectors that record the incoming and transmitted intensities. To improve the contrast of these measurements, high-Z contrast agents can be used. Such agents, however, can alter the fluid properties; high concentrations, in particular, can perturb the flowfield. It is especially difficult to separate the effects of composition and density gradients when both are present in a given flowfield.

We introduce X-ray fluorescence as an alternative X-ray technique for studying fluid mixing. While X-ray fluorescence is a widely used technique for elemental analysis (Beckhoff *et al.*, 2006), the authors are unaware of previous work using X-ray fluorescence to probe turbulent fluid mixing. Unlike radiography measurements, the fluorescence signal is, after the application of corrections, directly proportional to both the incident beam intensity and the amount of a given element in the X-ray beam path. Thus, fluorescence measurements have the potential for less corruption by noise than radiography, particularly for weakly absorbing samples. Robert *et al.* (1999) demonstrated the use of UV fluorescence in gas jet flowfields, but such measurements are subject to the same absorption problems as visible light techniques in optically dense media.

In this work we compare X-ray fluorescence and X-ray radiography of single-phase turbulent jets. Different concentrations of the fluorescent species are used to explore the ability of the technique to work at relatively low concentrations. The measurements are also compared with literature measurements of single-phase jets.

2. Experimental set-up

These experiments were performed at the 7BM beamline at the Advanced Photon Source, Argonne National Laboratory. Bending-magnet radiation passed through a double multilayer monochromator ($\Delta E/E = 1.4\%$) and was focused using a pair of 300 mm-long mirrors in a Kirkpatrick–Baez geometry at 6 mrad nominal grazing angle. The measured focus spot of the X-ray beam was 5 μm × 6 μm FWHM. The photon energy of the X-ray beam was 7 keV, with an incident flux at the focus of roughly 2×10^{10} photons s^{-1}.

We chose argon as the fluorescent element in the current experiments. Argon suffers from numerous disadvantages as an X-ray fluorescence tracer: relatively low fluorescence efficiency, moderate photoelectric cross section, low $K\alpha$ photon energy, and ubiquitous background argon in the atmosphere. However, argon is readily available and its K-edge can be excited with relatively low X-ray energies (>3.2 keV). The physical properties of argon are also closer to those of air than other potential gaseous tracer elements, such as krypton or xenon. Finally, argon is commonly used as a diluent gas in

Table 1
Flowfield parameters.

Orifice diameter	1.23 ± 0.02 mm
Orifice length	10 mm
Ambient pressure	98 kPa
Gas stagnation temperature	299 ± 1 K
Jet Reynolds number	2000, 15000

applied combustion experiments, one of the anticipated uses of this diagnostic.

The experimental apparatus consisted of a free round turbulent jet placed at the beam focus. Important parameters of the experiments are given in Table 1, and a schematic of the experimental set-up is shown in Fig. 1. The jet was produced by a long tube terminated by a sharp-edged orifice. The coordinate system is shown in Fig. 1; the x direction is along the jet axis, with $x = 0$ corresponding to the jet exit, while the y axis is transverse to the jet axis. The apparatus was raster scanned in the x and y directions across the X-ray beam to provide two-dimensional mappings of the jet mixing from x = 0.2 mm to x = 40 mm, which encompasses the entire development from the jet exit until self-similar behavior is expected (Pope, 2000). The jet was directed to a high-capacity exhaust system mounted 50 cm above the jet exit.

Measurements were performed for two gases: pure argon and a mixture of 10% argon by volume in nitrogen. The jets are characterized by the jet Reynolds number, defined as

$$\mathrm{Re} = \frac{\rho V d}{\mu} = \frac{4\dot{m}}{\pi d \mu}, \qquad (1)$$

where $\dot{m}$ is the jet mass flow rate, d is the jet diameter, ρ is the jet density, V is the jet velocity and μ is the jet fluid viscosity. The jet mass flow rate was measured using a thermal mass flowmeter with ±2% accuracy. The variations in measured mass flow rate during the experiment were approximately ±2% of the steady-state flow rate. The jet stagnation temperature was monitored using a T-type thermocouple (±1 K). The jet stagnation pressure was monitored using an absolute pressure transducer (±0.5 kPa). Flow velocities ranged from 20 m s^{-1} for the Re = 2000 argon jet to 190 m s^{-1} for the Re = 15000 jet of 10% argon. For the Re = 15000 jets, compressibility effects may also be present (jet Mach number = 0.5–0.6), but are expected to be minor.

Two simultaneous measurements were performed in this experiment. The X-ray absorption of the jet was measured with an ion chambers (I0) and an unbiased PIN diode (transmitted beam). The signals from both absorption detectors were directed to transimpedance amplifiers. The resulting voltage signal was converted to a frequency signal and recorded with a scaler counter.

The fluorescence was recorded with a Vortex silicon drift diode (SDD) of 50 mm^2 active area, placed approximately 42 mm from the beam focus. The SDD was oriented 90° from the beam in the synchrotron plane to minimize the elastically scattered flux received by the diode. The signal from the SDD was directed to a digital signal-processing unit to convert the signal to photon energy. An example spectrum from the 10% argon jet is shown in Fig. 2. The argon fluorescence photons at 3 keV are well separated from both the elastically scattered photons near 7 keV and the fluorescence from the chromium and manganese present in the nozzle (5.4 and 5.9 keV, respectively). A region of interest (ROI) was defined to include both the argon $K\alpha$ and $K\beta$ fluorescence lines. For each measurement point the signal was integrated for all detectors for either 5 s (100% argon jet) or 10 s (10% argon jet).

Several corrections were performed to the raw data to obtain the argon distribution in the jet. The absorption data were normalized by the X-ray transmission far outside the jet. The fluorescence data were normalized using the I0 ion chamber readings and corrected for spectral background using the measured intensity at photon energies slightly outside the argon fluorescence ROI. To correct for detector dead-time effects, the fluorescence signal was multiplied by the ratio of the input count rate to output count rate of the Vortex signal processor (Walko *et al.*, 2010); the detector dead-time was less than 4% in all cases. The background owing to ambient argon was removed using a scan performed with no flow from the jet.

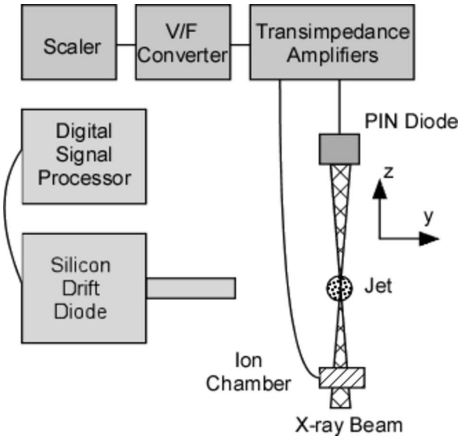

Figure 1
Experimental set-up. The x axis, *i.e.* the direction of jet flow, is directed out of the page.

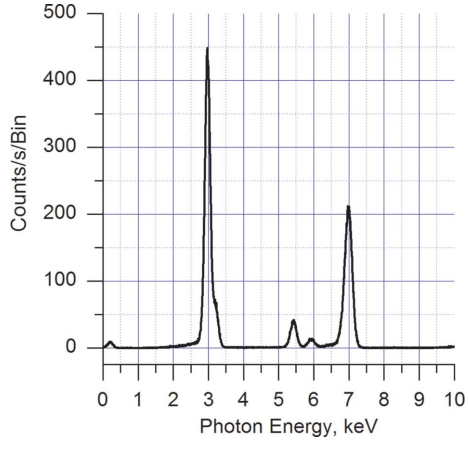

Figure 2
Example spectrum from the silicon drift diode. Data for 10% argon jet, x = 0.2 mm, y = 0 mm. The vertical axis gives counts s^{-1} in each 5 eV-wide energy bin of the processed data.

The intensity of this background was approximately 25% of the peak intensity of fluorescence from the 100% argon jet. The fluorescence signal was also corrected for absorption of fluorescent photons by the ambient air and the self-absorption of the primary X-ray beam in the jet (using the absorption measurement); this self-absorption of the primary X-ray beam was quite minor, as discussed below.

3. Results

As a first step we calibrate the fluorescence data with simultaneously collected absorption data (which are easier to interpret) for a relatively strongly absorbing case. A comparison between the absorbed photon flux and the total fluorescence photon flux for the Re = 2000 jet of 100% argon is shown in Fig. 3. These data represent over 2000 individual measurements ranging from x = 0.1 to 38 mm. The trend is quite linear, validating that the fluorescence measurements correlate well with the absorption measurements. A linear fit to the data in Fig. 3 shows that the conversion efficiency of absorption into fluorescence is approximately 9%. This is somewhat lower than the literature value of 12% (Hubbell *et al.*, 1994). This discrepancy may be caused by errors in the distance of the SDD from the jet, which strongly influences the collected solid angle; an error of 5–6 mm in the distance from the active surface of the SDD to the jet would explain the discrepancy from the literature value. The results for the Re = 15000 jet of 100% argon are virtually identical.

The advantages of the fluorescence technique compared with absorption become apparent for a dilute argon jet. Fig. 4 compares the absorption and fluorescence measurements for a scan perpendicular to the jet axis 20 mm from the nozzle exit. The absorption measurements show a much larger degree of noise than the fluorescence measurements, owing to the fact that the maximum absorption for this scan is less than 0.4%. To achieve a signal-to-noise ratio (S/N) of 10 in a pathlength calculation from absorption measurements, the X-ray intensity must be measured to an accuracy greater than 1 part in 1000. For the fluorescence data the main source of noise is photon shot noise. Once the background owing to atmospheric argon is taken into account, a S/N in the raw data of 50 is sufficient to achieve a S/N of 10 in the pathlength, which is quite feasible. We estimate that measurements at 5% argon concentration would be possible with the current experimental set-up, with lower yet adequate S/N.

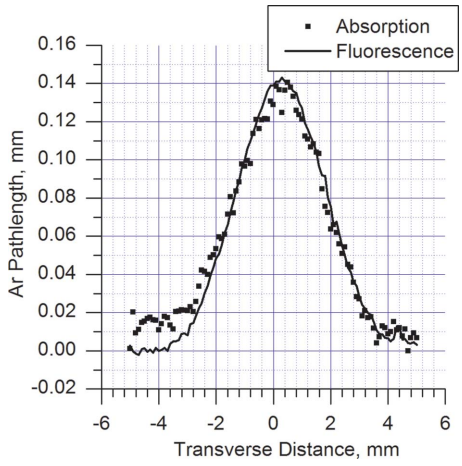

Figure 4
Comparison of radiography and fluorescence for a pure argon jet, Re = 2000, 20 mm from the jet exit.

We next use the fluorescence measurements to study the behavior of turbulent single-phase jets. As shown in Fig. 5, the shapes of the distributions are similar for various x. For easier comparison to literature data, x is normalized by the nominal nozzle diameter d; moreover, to account for the linear spread of the jet, the transverse coordinate y is normalized by x. This self-similarity is the expected behavior of turbulent jets far from the nozzle. Compared with the model for jet concentration distribution given by So *et al.* (1990), the current data show a slightly narrower distribution but otherwise match the

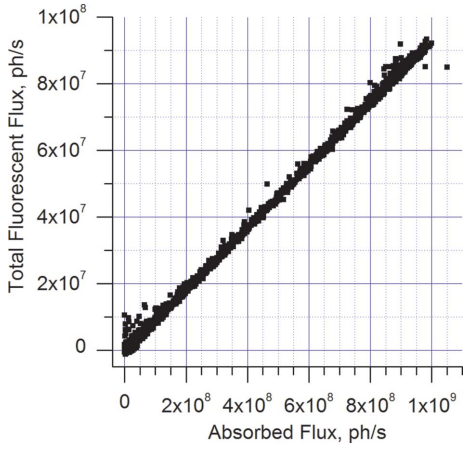

Figure 3
Comparison of absorbed flux to total fluorescence signal. The fluorescence signal has been converted to a flux over 4π steradians using the known SDD active area.

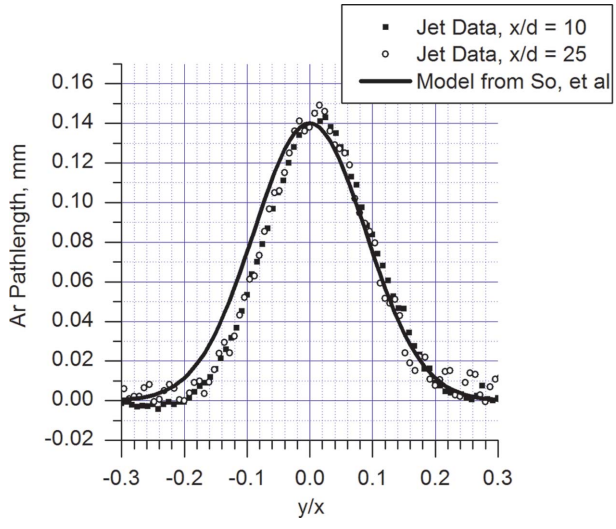

Figure 5
Distributions of argon pathlength perpendicular to the jet axis and the model given by So *et al.* (1990) for the 10% argon jet.

data quite well. The measured spreading rate of the jet (0.2 ± 0.05 when referenced to the FWHM of the argon distribution) for $x/d > 10$ is consistent with the accepted spreading rate of single-phase turbulent jets (Pope, 2000; So *et al.*, 1990).

The two-dimensional data collected in this study can also be used to visualize the jet structure. Fig. 6 shows the argon concentration (in terms of the pathlength of argon gas in the beam path) derived from the fluorescence measurements for the Re = 2000 and Re = 15000 jets of 100% argon. In the farthest downstream regions, both jets demonstrate a linear spreading rate, as expected from literature measurements of turbulent jets. The development of the jet in the first 10 mm from the nozzle is much slower for the Re = 2000 jet compared with the Re = 15000 jet. This indicates a significant dependence of the near-nozzle jet structure on the inlet conditions, which has been seen in literature measurements of low-Re jets (Kwon & Seo, 2005).

Finally, we apply the fluorescence data we have acquired by comparing the behavior of the current gas jets and previous data of liquid sprays (Kastengren *et al.*, 2009). In our previous radiography measurements of sprays from orifice nozzles, the X-ray absorption on the spray axis decreased sharply with downstream distance. In contrast, in the current gas jets, the absorption and fluorescence on the jet axis are almost constant with downstream distance, as seen in Fig. 6. A comparison of

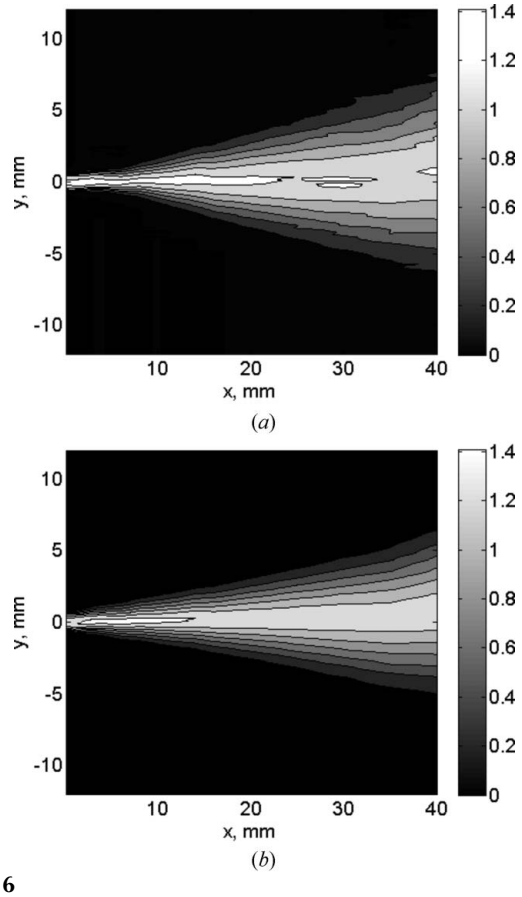

Figure 6
Distribution of argon pathlength (in mm) at ambient pressure and temperature in 100% Ar jet at (*a*) Re = 2000 and (*b*) Re = 15000. Each contour line represents 0.2 mm pathlength increments.

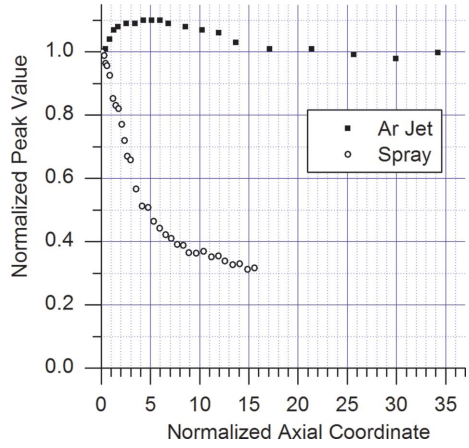

Figure 7
Comparison of pathlength-integrated values on the jet axis for the 100% Ar jet at Re = 15000 and a liquid spray at approximately Re = 15000, measured with X-ray fluorescence and absorption, respectively.

the centerline jet concentration between a single-phase jet and a spray is shown in Fig. 7. The spray data are from a 110 µm-diameter orifice injecting liquid with 840 kg m^{-3} density into a 22.5 kg m^{-3} ambient gas at approximately Re = 15000; the single-phase jet data are for the current 100% argon jet at Re = 15000. For both datasets the axial coordinate has been normalized with the nozzle diameter and density ratio between the jet and ambient gas (Kastengren *et al.*, 2009); the vertical coordinate has been normalized by the measured value at the nozzle exit. Previous measurements of single-phase jets have shown that the jet width increases linearly with downstream distance, while the jet concentration is inversely proportional to downstream distance (Pope, 2000; So *et al.*, 1990). As such, the current data and the example spray data, which are pathlength integrated, should be constant with downstream distance. This matches the behavior seen in the current single-phase jet, but not the spray data.

There are three possible explanations for the differences in behavior of the two flowfields. The first is that the spray case has a much higher density ratio between the jet and ambient fluids than the current gas jet experiments; while methods exist to account for density ratio effects (Pitts, 1991), these methods have generally been developed using gas jet data at lower density ratio values than in the spray case shown in Fig. 7. The second is due to surface tension effects. Owing to the production of discrete droplets, mixing in a spray is expected to be different than in a single-phase jet at small scales. Perhaps this process also alters the mixing at larger scales. Finally, the viscosity of the ambient gas is much lower than that of the liquid in a spray. Perhaps this difference in viscosity also plays a role in the mixing near the nozzle. More study is needed to understand which of these mechanisms is correct.

4. Conclusions

X-ray fluorescence has been used to measure the mixing of single-phase turbulent jets. The fluorescence measurements

are well correlated with X-ray absorption measurements. The fluorescence measurements demonstrate less noise and susceptibility to drift than the absorption measurements and agree closely with the accepted behavior of single-phase turbulent jets. These data show that X-ray fluorescence can be effectively used as an X-ray diagnostic for fluid flows with weak X-ray absorption. The ability to seed a fluid stream with fluorescent tracer and track mixing in optically dense environments could provide important insights in several flowfields, including non-premixed flames and two-fluid impinging jet atomizers.

This research was performed at the 7BM beamline of the Advanced Photon Source, Argonne National Laboratory. The submitted manuscript has been created by UChicago Argonne, LLC, Operator of Argonne National Laboratory ('Argonne'). Argonne, a US Department of Energy Office of Science laboratory, is operated under Contract No. DE-AC02-06CH11357.

References

Beckhoff, B., Kanngiesser, B., Langhoff, N., Wedell, R. & Wolff, H. (2006). *Handbook of Practical X-ray Fluorescence Analysis.* Berlin: Springer.

Hubbell, J. H., Trehan, P. N., Singh, N., Chand, B., Mehta, D., Garg, M. L., Garg, R. R., Singh, S. & Puri, S. (1994). *J. Phys. Chem. Ref. Data*, **23**, 339–364.

Kastengren, A., Powell, C. F., Wang, Y.-J., Im, K.-S. & Wang, J. (2009). *Atomization Sprays*, **19**, 1031–1044.

Kuo, K. K., Hsieh, K. C. & Char, J. M. (1990). *J. Propul. Power*, **6**, 544–551.

Kwon, S. J. & Seo, I. W. (2005). *Exp. Fluids*, **38**, 801–812.

MacPhee, A. G., Tate, M. W., Powell, C. F., Yue, Y., Renzi, M. J., Ercan, A., Narayanan, S., Fontes, E., Walther, J., Schaller, J., Gruner, S. M. & Wang, J. (2002). *Science*, **295**, 1261–1263.

Pitts, W. (1991). *Exp. Fluids*, **11**, 125–134.

Pope, S. (2000). *Turbulent Flows.* Cambridge University Press.

Robert, E., Huré, L., Cachoncinlle, C., Viladrosa, R. & Pouvesle, J. (1999). *Meas. Sci. Technol.* **10**, 789–795.

Sick, V. & Stojkovic, B. (2001). *Appl. Opt.* **40**, 2435–2442.

So, R. M. C., Zhu, J. Y., ÖtüGen, M. V. & Hwang, B. C. (1990). *Exp. Fluids*, **9**, 273–284.

Walko, D. A., Arms, D. A., Miceli, A. & Kastengren, A. (2010). *Nucl. Instrum. Methods Phys. Res. A.* In the press (doi:10.1016/j.nima.2010.12.059).